Applied Mathematical Modelling 37 (2013) 3181–3192

Contents lists available at SciVerse ScienceDirect

Applied Mathematical Modelling

journal homepage: www.elsevier.com/locate/apm

Measuring heat transfer during spray cooling using controlled induction-heating experiments and computational models

Xiaoxu Zhou [a,1], Brian G. Thomas [a,*], C. Alberto Hernández B. [b], A. Humberto Castillejos E. [b], F. Andrés Acosta G. [b]

[a] Department of Mechanical Science and Engineering, University of Illinois at Urbana-Champaign, 1206 West Green Street, Urbana, IL 61801, USA
[b] Centre for Research and Advanced Studies, CINVESTAV-Unidad Saltillo, Carr. Saltillo-Monterrey Km. 13.5, Saltillo, Coahuila 25900, Mexico

ARTICLE INFO

Article history:
Received 9 October 2011
Received in revised form 14 July 2012
Accepted 20 July 2012
Available online 16 August 2012

Keywords:
Spray-cooling
Induction heating
Electromagnetics
Heat transfer
Finite-element model
Measurement method

ABSTRACT

This paper presents a methodology combining experimental measurements with computational modeling to find the heat flux extracted during spray cooling of a metal surface. Controlled experiments are performed to impinge air-mist spray onto a metal probe surface while applying induction heating to follow a desired temperature history. A transient axisymmetric computational model of induction heating which couples electromagnetics and heat conduction has been developed and validated with a test problem. The model is calibrated to match transient dry measurements and then used to simulate a steady-state air-mist spray cooling experiment in order to quantify the heat extracted from the probe surface by the boiling water droplets. A detailed example is presented to illustrate this approach.

1. Introduction

Spray-cooling is widely applied in many industrial processes, including metal production, heat treatment, emergency cooling systems, power-generation, and electronic-component cooling. It is characterized by good uniformity and a wide range of heat removal rates, including extremely high heat transfer. It is important to quantify the spray heat transfer rates for various conditions and different material surface temperatures in order to better control the spray-cooling applications.

To obtain a heat transfer rate always requires the use of mathematical modeling to extract the results from the experimental measurements. Several previous studies have used simple analytical models to extract spray heat transfer rates from measurements involving preheating and simple geometries. Moriyama et al. [1] preheated a cylindrical metal block to 300–450 °C, cooled the surface with impinging water droplets, and calculated transient heat transfer coefficients with an analytical solution for two-dimensional axisymmetric heat transfer. Timm et al. [2] calculated heat flux for jet impingement at high wall temperatures by analytically solving momentum, continuity and heat transfer equations.

Many experiments cool a preheated sample, and extract heat transfer coefficient histories using numerical transient heat conduction models. For example, Horsky et al. and Raudensky et al. [3,4] used a numerical one-dimensional inverse transient heat conduction model [5] to calculate spray heat flux in transient cooling experiments on a preheated austenitic steel plate. Choi and Yao [6] preheated a cylindrical copper plate to ~450 °C, spray-cooled it, and solved a numerical one-dimensional

* Corresponding author. Tel.: +1 217 333 6919; fax: +1 217 244 6534.
E-mail addresses: xiaoxu.zhou@ssab.com (X. Zhou), bgthomas@illinois.edu (B.G. Thomas), constantin.hernandez@cinvestav.edu.mx (C.A. Hernández B.), humberto.castillejos@cinvestav.edu.mx (A.H. Castillejos E.), andres.acosta@cinvestav.edu.mx (F.A. Acosta G.).
[1] Present address: SSAB Research & Development Facility, 1755 Bill Sharp Blvd, Muscatine, IA 52761, USA.

0307-904X/$ - see front matter © 2012 Elsevier Inc. All rights reserved.
http://dx.doi.org/10.1016/j.apm.2012.07.039

transient heat conduction inverse model for spray heat fluxes for various horizontal jet conditions. Kumagai et al. [7] used a burner to heat up a rectangular copper block and then cooled it using water spray. The transient surface heat flux was calculated based on curve fitting the temperatures of four thermocouple measurements in the copper block. Sozbir et al. [8] preheated a stainless steel plate, spray-cooled it with water, and calculated heat flux by solving the lumped heat transfer equation for a thin plate. In these transient experiments with spray-cooled preheated samples, heat transfer coefficients change with both the metal surface temperature and time, so it is not possible to isolate and study these two different effects independently.

Supplying heat to the sample during cooling can overcome this problem. Bernardin and Mudawar [9,10] used three electrical cartridge heaters to heat a thin cylinder nickel plate up to 400 °C while being cooled by single and multiple impinging droplet streams, and then extrapolated a one-dimensional temperature curve fit of temperatures recorded by four thermocouples to determine the plate surface temperature and surface heat flux histories. This method requires a large sample and many thermocouples. Graham and Ramadhyani [11] used a DC-powered resistance heater to heat a copper cube ($6.35 \times 6.35 \times 6.35$ mm^3) while cooling it with air-mist impingement. Average heat flux was estimated simply from the total resistance heating power per unit area of sample surface. This simple model requires a very thin sample, uniform heat source distribution, and perfect insulation of the side and back surfaces.

Puschmann et al. [12] and Schmidt et al. [13] used DC power supply to heat a metal plate while cooling it with water spray, and used infrared thermal imaging to measure the surface temperature. Spray heat transfer coefficients were calculated based on an analytical heat balance of the total supplied heat, resistance heat and the heat taken away by the spray. Robidou et al. [14] used a metallic resistance foil to heat a piece of pure copper while it was water spray-cooled, and found local heat fluxes by solving a two-dimensional inverse heat conduction problem. In these spray cooling experiments, DC power supplies or electrical heaters limit the power delivered to surface temperatures less than 900 °C.

Induction heating enables spray cooling experiments where the temperature histories are controlled as desired to study fundamental behaviors during steady-state, or to follow realistic paths found in commercial operations. The heat transfer phenomena are complicated, however, due to electromagnetic heat sources, thermal diffusion with high spatial gradients, and external water cooling. This makes the measurements difficult to interpret without the aid of an advanced computational model. Many researchers [15–23] have applied two or three-dimensional finite-element models to solve induction heating problems. The numerical methods to incorporate induction heating problems are now well developed and integrated into several commercial software packages such as ANSYS [24] and COMSOL [25].

The present project introduces a methodology to measure heat transfer coefficients during spray cooling using a controlled induction heating experiment and a detailed computational model of this experiment. With the laboratory apparatus, a small cylindrical platinum sample is spray-cooled from a commercial air-mist nozzle, while induction heating is applied to balance the heat removal to maintain a setpoint temperature. Because the sample can be moved to any desired location in the spray, it is referred to as a ''probe''. A two-dimensional axisymmetric model of this apparatus that couples electromagnetics and heat transfer is developed in COMSOL, validated with previous solutions, calibrated with transient induction heating experiments, and finally applied to extract the heat transfer rates from spray-cooling experimental measurements. An example is presented for a steady experiment at a thermocouple temperature of 700 °C. This methodology of combining induction heating experiments and computational modeling provides a fundamental tool to quantify heat transfer during spray cooling for a wide range of conditions and surface temperatures (85–1200 °C).

2. Experiments

The new experimental apparatus to measure heat transfer during spray cooling with induction heating has been developed at the Laboratory of Process Metallurgy at CINVESTAV, Mexico, as shown in Fig. 1. A 4 mm (radius) × 2.5 mm (height) cylindrical platinum (Pt) probe is positioned inside a two-loop copper coil, (right of Fig. 1). The probe and the coil are cast into a cylindrical ceramic body. The Pt probe is mounted just behind a hole in a large thin transparent quartz plate which acts as the vertical impingement surface, oriented perpendicular to the water spray. Water or air-mist spray from the nozzle impinges directly onto the plate and the exposed front surface of the probe, while it is simultaneously heated internally by induction from a water-cooled induction copper coil. Power is adjusted continuously to maintain the desired temperature

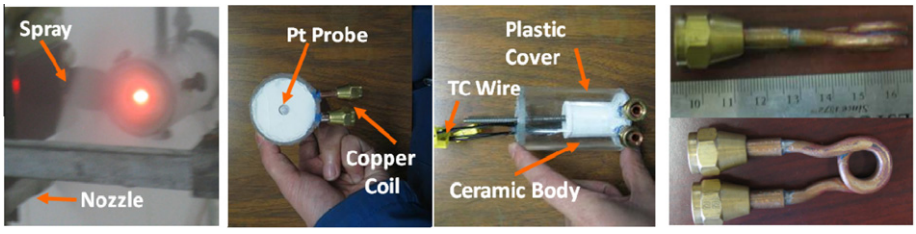

Fig. 1. Experimental apparatus, assembled ceramic body and copper induction coil.

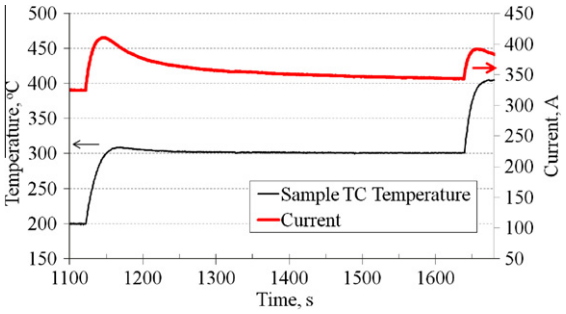

Fig. 2. Typical wet experiment measurements: TC temperature and total current.

of a thermocouple (TC) that is attached to the back surface of the probe. A large flat plastic cover protects the ceramic body from the spray. The total current through the coil is recorded.

The system can be programmed to reproduce any desired temperature profile, such as matching the real surface temperature history experienced by a point on the surface of the steel strand as it moves through a continuous casting machine. An example of the experimental measurements is shown in Fig. 2, for the sample TC temperature setpoint suddenly increased to 300 °C from a previous 200 °C steady-state condition. The probe is oriented along the axis of a Delavan W19822 air-mist spray nozzle to measure the case of maximum cooling, for a setback distance of 0.19 m. The induction heating control system increases the power delivered to the probe to stabilize the probe TC measurement at 300 °C, which takes a few minutes. The corresponding current measurement overshoots and then gradually decreases to stabilize at 350 A, which takes about 8 min.

In order to provide additional data needed for model calibration, a series of "dry" experiments were also performed, where the spray is turned off and the surface temperature setpoint is increased in steps of 100 °C from 100 to 1200 °C. Further details of this experimental system and its results are given elsewhere [26].

3. Model development

A two-dimensional, axisymmetric finite-element model of the induced electromagnetic field and transient heat transfer in the experimental spray-cooling system has been developed to extract heat transfer coefficients from the measurements. The high-frequency varying magnetic field induces eddy currents inside the Pt probe and the coil and generates resistance heating, which is extracted by the coil cooling water and the environment, in addition to the air-mist spray. The small probe of the present system enables easy handling, high temperatures, fast response, and good control. However, it can accommodate only one thermocouple. Thus, a sophisticated computational model is required to quantify the complex electromagnetics and transient heat transfer phenomena associated with this experiment.

3.1. Governing equations

The following electromagnetics equation [15–23] is solved for the amplitude of the magnetic vector potential, **A** (V s/m), with isotropic material properties and an externally-applied sinusoidally-varying current I_{ext} ($\int\int_{area}\mathbf{J_{ext}}exp(i\omega t)\cdot d\mathbf{a}$):

$$\nabla^2\mathbf{A}+\omega^2\mu\varepsilon\mathbf{A}=j\mu\omega\sigma\mathbf{A}-\mu\mathbf{J_{ext}} \tag{1}$$

where ω is angular frequency of the external alternating current (rad/s); μ is magnetic permeability (V s/A m), ε is the permittivity (s/m ohm), σ is the temperature-dependent electrical conductivity (1/m ohm) and **a** is cross-section area (m^2). The current density vector $\mathbf{J_{ext}}$ (A/m^2) in the two-dimensional axisymmetric problem is simply $J_{ext\theta}\mathbf{e_\theta}$. The vector potential **A** is thus $A_\theta\mathbf{e_\theta}$ because the other components $J_{extr}\mathbf{e_r}$ and $J_{extz}\mathbf{e_z}$ are zero. (Note: $\mathbf{e_r}$, $\mathbf{e_\theta}$, $\mathbf{e_z}$ are orthogonal unit vectors in cylindrical coordinates). Eq. (1) is thus simplified into the following two-dimensional axisymmetric scalar equation

$$\frac{1}{r}\frac{\partial}{\partial r}\left(r\frac{\partial A_\theta}{\partial r}\right)+\frac{\partial^2 A_\theta}{\partial z^2}+\omega^2\mu\varepsilon A_\theta=j\mu\omega\sigma A_\theta-\mu J_{ext\theta} \tag{2}$$

With the external current in the coil of the experimental system having a frequency ($\omega/2\pi$) of 2.53×10^5 Hz, the third term on the left side of Eq. (2) can be neglected because:

$$|\omega^2\mu\varepsilon|\ll|j\mu\omega\sigma| \tag{3}$$

The model also solves the two-dimensional transient heat conduction equation for the temperature, T, throughout the ceramic body domain as a function of time, t:

$$\rho C_p\frac{\partial T}{\partial t}=\frac{1}{r}\left(\frac{\partial}{\partial r}rk(T)\frac{\partial T}{\partial r}\right)+\frac{\partial}{\partial z}k(T)\frac{\partial T}{\partial z}+Q(T,\mathbf{J_{tot}}) \tag{4}$$

where ρ is density (kg/m^3), C_p is specific heat (J/kg K), and k is the temperature-dependent thermal conductivity, (W/m K), and the heat source Q (W/m^3) is from resistance heating:

$$Q = \frac{|\mathbf{J_{tot}}|^2}{2\sigma(T)} \tag{5}$$

where the total current density, $\mathbf{J_{tot}}$ ($J_{tot\theta}\mathbf{e_\theta}$), is the sum of the induced eddy current density and the external applied current density, $\mathbf{J_{ext}}$, and is found by rewriting Eq. (2) as follows:

$$J_{tot\theta} = -j\omega\sigma(T)A_\theta + J_{ext\theta} = -\frac{1}{\mu}\left(\frac{1}{r}\frac{\partial}{\partial r}\left(r\frac{\partial A_\theta}{\partial r}\right) + \frac{\partial^2 A_\theta}{\partial z^2}\right) \tag{6}$$

This full expansion is only needed in the coil region. In the Pt probe, $J_{ext\theta}$ is 0, and elsewhere in the air and ceramic body, $J_{tot\theta}$ is 0.

3.2. Model domain and boundary conditions

Fig. 3 shows the two-dimensional axisymmetric domain of the spray-cooling apparatus, including the ceramic body, induction copper coil, probe, air and quartz plate, geometry dimensions, and boundary conditions. The domain for the electromagnetics equation includes a surrounding air volume that is 13× larger than the ceramic body. This large domain was chosen to ensure that the magnetic potential is approximately zero at the three far-away boundaries. The domain for the heat conduction equation is limited to the ceramic, copper, and probe (shaded regions). Axial symmetry is assumed in both problems about the centerline.

For the heat transfer problem, the boundary conditions included both convection and radiation,

$$q = -k\partial T/\partial n = h(T - T_a) + \sigma_{SB}e(T^4 - T_a^4) \tag{7}$$

where n is the unit-normal to the surface, σ_{SB} is the Stefan–Boltzmann constant, 5.67 × 10^{-8} W/m^2 K^4, e is the effective emissivity, h is h_{cw}, h_{nat}, h_{spray} and h_{front}, in the different regions of the ceramic-body surface, and T_a is the ambient air or water temperature. A forced convective heat transfer coefficient at the copper coil interface with the cooling water, h_{cw}, was estimated with the empirical relationship from Sleicher and Rouse, given in [27], based on the coil surface temperature, cooling water temperature, and cooling water velocity. A natural convective heat transfer coefficient h_{nat} of 10 W/m^2 K is used at the top and right boundaries, which has little influence relative to the large heat removal by the spray and cooling water.

The front surface of the Pt probe is exposed to the spray water–air mist cooling. A forced convective heat transfer coefficient h_{spray} is selected for this surface by trial and error to make the temperature prediction at the thermocouple location match the measurement. Spray also impacts onto the quartz surface, where a forced convective heat transfer coefficient, h_{front}, is estimated using the empirical correlation by Nozaki [28] with the coefficient A = 1.

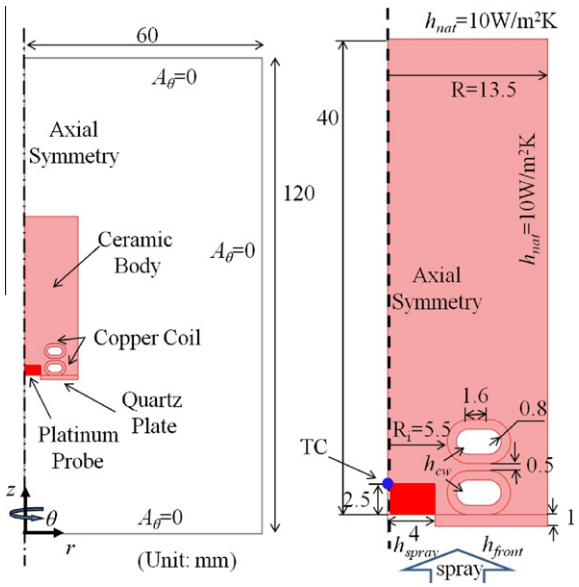

Fig. 3. Model domain and boundary conditions for electromagnetics (left) and heat transfer (right).

$$h_{front}(W/m^2K) = A * 1570 * Q_w^{0.55}(l/m^2s)(1 - 0.0075T_a(^\circ C)) \quad (8)$$

where Q_w is the measured impact spray water flow rate on the quartz surface, and T_a is the ambient temperature of the spray water and air. Uncertainty in this estimation arises from the inaccuracy of the correlation, the different nozzle orientation and the measurement of impact spray water flow rates. Therefore, a parametric study of h_{front} was performed and will be discussed later.

In the dry tests, both h_{spray} and h_{front} represent the natural convection coefficient with the ambient air, which is estimated to be 10 W/m^2 K. In addition, thermal radiation, the second term on the right hand of Eq. (7), is added to all of the natural convection boundaries. In contrast with the high and uncertain spray heat extraction rates in the wet experiments, the dry experiments involve small, well-characterized natural convection and radiation boundary conditions which permit accurate model calibration.

3.3. Material properties

Electrical and thermal properties for the platinum [29] and other materials are listed in Table 1 and Pt emissivity [29] in Table 2. The ceramic thermal conductivity k_{cer} varies with ceramic temperature and porosity and is obtained via calibration of the dry experiment. The permeability and permissivity for all the materials are constant 1.3×10^{-6} V s/A m and 8.85×10^{-12} s/m ohm.

3.4. Numerical details

The Galerkin finite-element method was applied to spatially discretize the equation system, Eqs. 2 and 4, which are fully coupled via T and $\mathbf{J_{tot}}$. The solution procedure is outlined in Fig. 4. Temperature T and $\mathbf{J_{ext}}$ from the time step t_n are taken as initial guesses to start the next time step t_{n+1}. Then Eqs. 2 and 4 are solved for nodal temperatures, $T(r, z)$, and potentials, $A_\theta(r, z)$, respectively. The predicted total current of the coil $\int\int_{area} \mathbf{J_{tot}} \cdot d\mathbf{a}$ is then evaluated by integrating Eq. (6) over the area of the coil, and compared with the total current measured in the experiment. Iteration continues until both T and $\mathbf{J_{tot}}$ converge

Table 1
Electrical and thermal material properties.

	Specific heat (J/kg K)	Density (kg/m^3)	Electrical conductivity (1/m ohm)	Thermal conductivity (W/m K)
Copper	385	8960	$5.7 \times 10^7/(1+0.0039(T\text{-}20))$	400 (25–150 °C)
Platinum	133	21,450	$9.6 \times 10^6/(1 + 0.0038(T\text{-}20))$	$71.86 + 0.0015T + 1.0118 \times 10^{-5}T^2$
Water	4187	988	0	—
Ceramic	740	1762	0	Obtained by model calibration
Quartz	755	2203	0	1.3

Table 2
Temperature-dependent platinum emissivity, e.

Temperature, °C	100	500	1000	1500
Emissivity	0.05	0.1	0.15	0.19

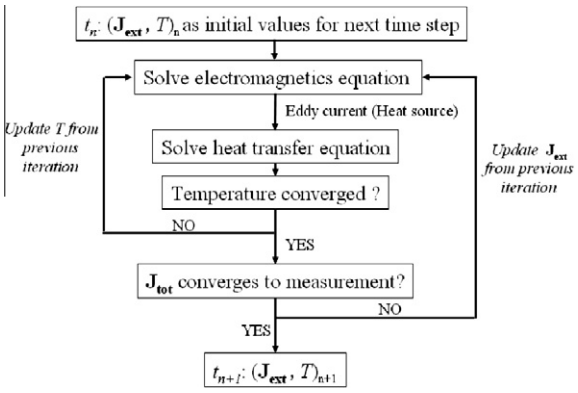

Fig. 4. Flow chart of solving coupled electromagnetics and heat transfer equations.

within 10^{-4}% residual error. To simulate a transient experiment, such as jumping from one temperature setpoint (T_i) to another (T_i + 100 °C), the solution is initialized with a steady-state simulation at the first temperature setpoint T_i, using the same solution procedure.

The computational domain in Fig. 3 was discretized into the same mesh of 11,968 standard 3-node axisymmetric triangular finite elements with 37,789 degrees of freedom for Eqs. 2 and 4. These simple elements are linear potential (constant current density) for Eq. (2) and linear temperature (constant heat-flux) for Eq. (4). A specially-refined mesh was applied around the copper coil and the probe to capture the high thermal gradients in this region, which is shown in Fig. 5. Further refinement of the mesh up to 39,701 elements found only a slight change in the results (<1% in the probe temperature) [30]. To save computational time, the coarser mesh was selected for the project.

For the transient Eq. (4), a variable time-stepping method, using the implicit three-level second-order BDF (backward differentiation formula) for temporal discretization, was applied with an initial time-step of 0.001 s increasing to a maximum of 0.1 s. The discretized finite-element equations were solved using direct Gaussian elimination in COMSOL [25], which required ~10 CPU min for each 100 s simulation with the 11,968-element mesh, using a 3.19 GHz Dell OPTIPLEX GX270 PC.

3.5. Model validation

To validate the internal consistency of the model and the mesh resolution, a simple one-dimensional axisymmetric transient induction heating problem [24] was solved. The domain is a 15 mm long, 1 mm thick strip along the radius of the long billet, as shown in Fig. 6 with the boundary conditions. Fig. 7 compares the current model results for a 180 × 3 mesh with previous work [24] for the temperature histories at points A and B. The two models match within 1%, which verifies the magnetic field and induction heating solution procedure.

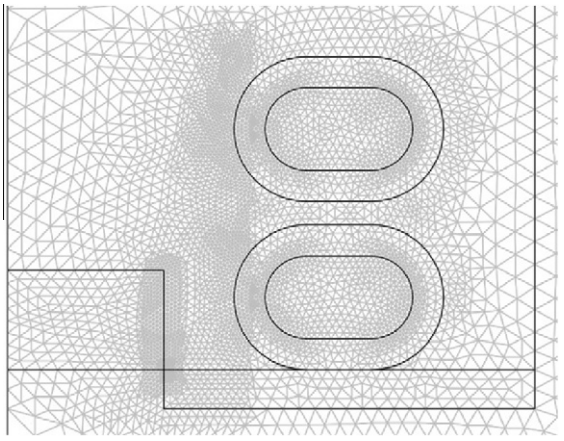

Fig. 5. Specially-refined mesh around the copper coil and the probe.

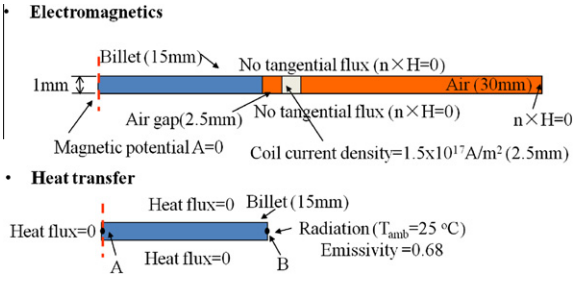

Fig. 6. Test problem domain and boundary conditions.

4. Error sensitivity studies

Parametric modeling studies were performed to determine the relative importance of different uncertainties on the results. Work presented elsewhere [31] finds that uncertainties in the RMS current, probe thickness, probe temperature, and off-center positioning of the thermocouple all amount to negligible (<2%) changes in the heat flux. Varying the quartz

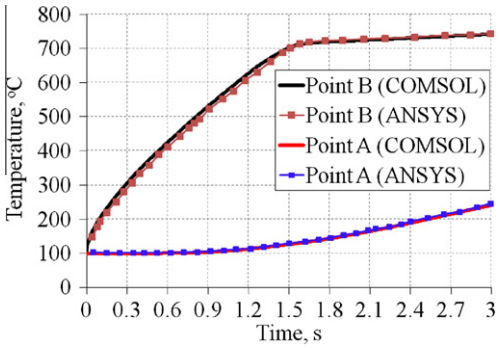

Fig. 7. Test problem temperature histories: comparing COMSOL and ANSYS models for point A and B.

surface boundary condition h_{front} over its estimated uncertainty range of 27%, changed the predicted spray heat transfer coefficient by less than 0.6%.

The size and shape of the probe disk and coils are more important. The gap size between the two copper coil loops was measured to vary from 0.4 to 0.6 mm. Using model domains with this range of different gap sizes, steady-state simulations found that heat generated inside the probe varies <3%; heat to the cooling water varies <1%, heat to the spray water varies <4%; and most importantly, spray heat transfer coefficient varies <3%. This result suggests that the variations and uncertainties in gap size do not change heat transfer much, so a typical gap size of 0.5 mm was assumed in later simulations.

5. Model calibration

Owing to inaccuracies in representation of the three-dimensional geometry with an axisymmetric two-dimensional model, calibration is needed to enable the model to predict the experiment accurately. As shown in Fig. 1, the complex, three-dimensional helical coil shape has two-loops over 70% of its circumference and one-loop over 30% as well as a straight tube portion, with a quasi-elliptical cross section. The axisymmetric model representation assumes two complete circular loops are used. To account for the over-prediction of heat induction caused by this inaccurate geometric assumption, the coil inner radius R_i (Fig. 3) was increased in order to decrease the total heat generated in the probe to match that of the real coil as closely as possible.

To determine how much to increase R_i, a parametric modeling study was performed with different R_i (5.0, 5.5, and 5.8 mm) for a fast transition in probe temperature from stable 700 °C to stable 800 °C in the dry experiment. For each R_i, the initial temperature distribution was obtained by matching the probe TC measurement at 700 °C in the steady state simulation. The measured current history for this temperature stage was input to the model. The transient probe TC temperature results and the measured current for this calibration step are shown in Fig. 8. The loop inner radius controls the heat generation which in turn controls the predicted transient temperature evolution shape. For an inner radius of 5.0 mm (real inner radius), the probe TC prediction jumps from 700 to 815 °C in 15 s, overshooting the measured temperature before dropping gradually to the steady temperature of 800 °C. As the coil inner radius increases, this unrealistic peak weakens. Smaller R_i gives larger overshoot while larger R_i gives longer transient time. As shown in Fig. 8, the 5.5 mm inner radius gives the best match with the measured transient temperature history.

In addition to R_i, ceramic thermal conductivity k_{cer} is also very important. Fixing the inner radius determines the heat generation. Then the prediction of probe TC temperature is controlled by k_{cer}. Increasing the conductivity takes away more heat through the ceramic and lowers the probe TC temperature. Thus, the transient model predictions were calibrated to match

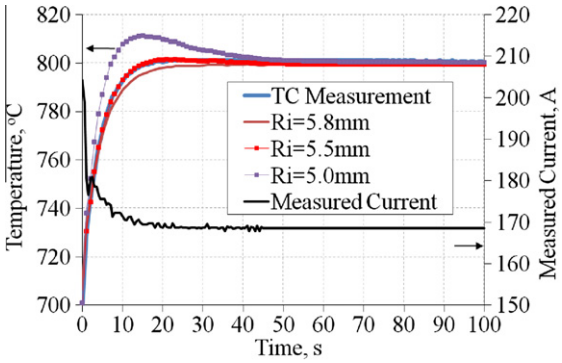

Fig. 8. Transient simulation of probe TC temperature for different coil loop inner radius (R_i).

the temperature histories generated in each of a sequence of incrementally-increased probe TC measurements in dry experiments to determine the best temperature-dependent k_{cer} function to use in all simulations.

Starting from a stable 100 °C probe temperature, the measured current from each dry experiment is input to the model and, k_{cer} is adjusted to make the prediction match the measurement. Repeating for each temperature increment to match k_{cer} at the highest temperature produces the calibrated temperature-dependent k_{cer} curve shown in Fig. 9. The model predictions and measurements of the probe TC temperature are shown in Fig. 10. They match well.

In order to check the validity of the calibrated temperature-dependent k_{cer}, a side experiment was performed. In this experiment, a cylindrical ceramic body with the same compositions as used in spray experiments rests on a thin metallic sheet, which is heated by a Bunsen burner. A TC is welded to the sheet to monitor the sheet temperature. Another eight TCs are installed along the axis of the ceramic body. The lateral surface is insulated with ceramic fiber. The top surface is exposed to natural convection. The experiment was continued for about 3 h while holding at a constant sheet temperature to make sure that the heat transfer inside the ceramic body had reached steady state. The TC measurements and the corresponding

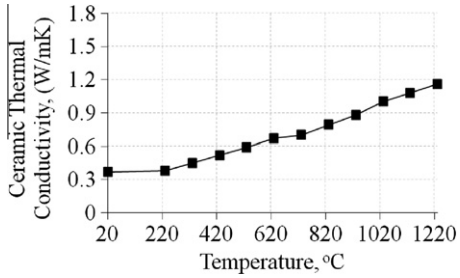

Fig. 9. Calibrated temperature-dependent ceramic thermal conductivity.

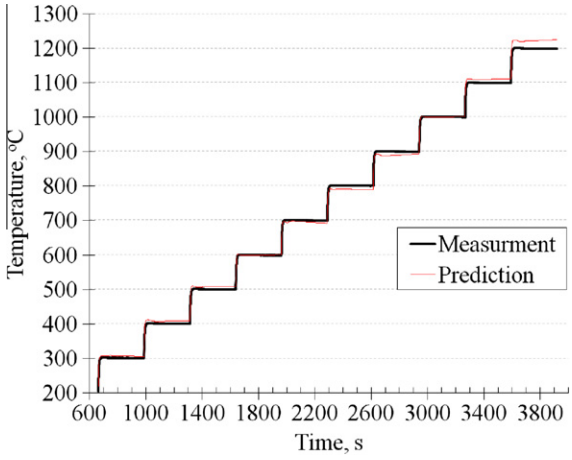

Fig. 10. Comparison between probe TC temperature measurements and predictions for the dry experiment.

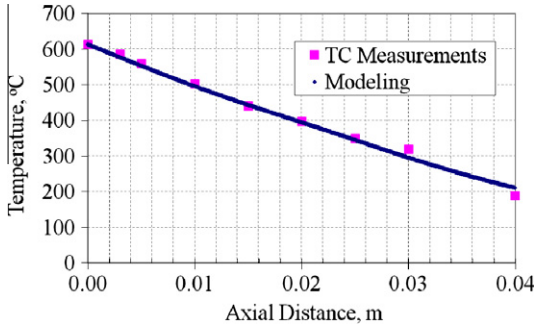

Fig. 11. Comparison of TC measurements and model predictions in the ceramic conductivity experiment.

simulation with the calibrated k_{cer} are shown in Fig. 11 to agree well. Thus, the calibrated R_i and temperature-dependent k_{cer} can be used in the model to simulate both transient and steady wet experiments.

6. Results and discussion

The model has been applied to measure heat transfer for a range of nozzles and cooling conditions [32]. As an example, the model is applied to extract the local heat flux at the probe front surface while spraying with the probe TC held stable at 700 °C. The Pt probe was centered along the spray nozzle axis to produce the maximum spray rate, with a water flow rate of 4.6 lpm and an air flow rate of 104 lpm. The input conditions for the model are listed in Table 3. The value of h_{spray} was adjusted until the temperature predicted at the TC location at the back of the probe matched the TC measurement (700 °C).

The model predictions also provide detailed insight into the experiment functioning. Fig. 12 shows the magnetic potential distribution calculated in the entire modeling domain. Magnetic potential is mainly confined to within the conductive materials and drops to zero far away towards the boundaries. The field is strongest in the left edges of the coil. As shown in the close-up, magnetic potential is much stronger near the right side surface (0.4 mm depth) of the Pt probe than elsewhere in this disk. Magnetic potential is difficult to penetrate into the Pt probe due to the well-known skin-effect.

Fig. 13 shows the total current density $\mathbf{J_{tot}}$ distribution inside both the copper coil and the Pt probe. Since no external current is applied inside the Pt disk (probe), only induced current exists. Induced current density is stronger at the right side near the induction copper coil. Since the bottom loop is closer to the Pt probe than the upper loop, the induced current density at the left side of the bottom loop is much stronger than that of upper loop. Induced current density is zero in the ceramic body, cooling water and the air, as they are nonconductive materials.

Table 3
Input parameters in the model.

Input	Heat transfer coefficient
Measured total current, A	484.6
h_{cw}, W/m^2 K	29,640
h_{front}, W/m^2 K	5500
h_{spray}, W/m^2 K	7100

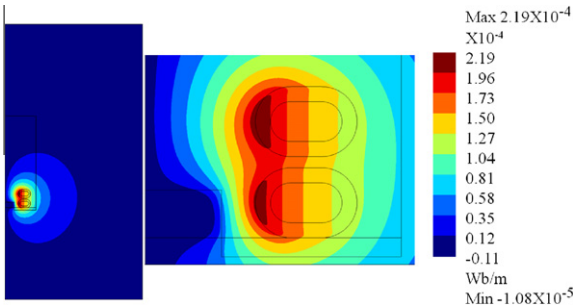

Fig. 12. Magnetic potential distribution: (left) entire domain; (right) close-up near bottom region of ceramic cylinder.

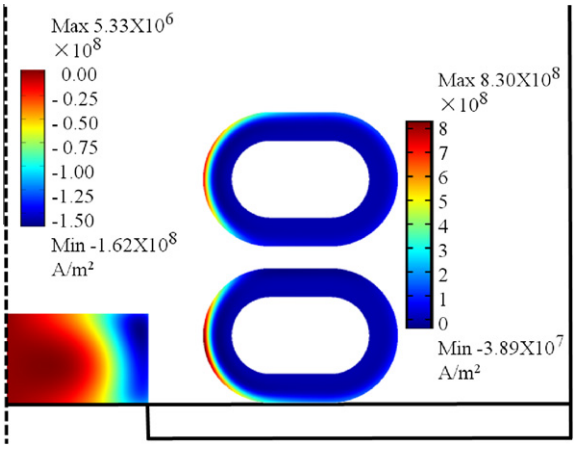

Fig. 13. Total current density ($\mathbf{J_{tot}}$) distribution inside the copper coil and the Pt probe.

Fig. 14 shows the heat source (power density distribution) generated by the total current inside the conducting regions. Heat is mainly generated in the surface layers (skins) of the induction coil and the Pt probe which are closest to each other. This power distribution is clearly consistent with the total current density distribution. Heat generated inside the probe is 264.49 W while that in the copper coil is 186.19 W. Heat generation is zero in the ceramic body and cooling water since they are nonconductive. The heat taken out by the cooling water through the tube is 206.22 W. The heat taken out from the front quartz window is 14.95 W and the heat taken away by natural convection is negligible, 0.44 W. The heat extracted by the spray cooling is 229.14 W which is obtained by integrating heat flux over the Pt surface. Naturally, the heat removed by the cooling water, spray water and natural convection is exactly balanced by the heat generated inside the Pt probe and the coil.

Fig. 15 shows the temperature distribution in the entire heat transfer domain. Temperature in the ceramic body deceases with distance away from the probe. Large temperature gradients are observed in the ceramic near the probe. The temperature inside the copper coil does not vary very much (~5 °C), which means it is reasonable to use constant material properties for each probe TC temperature simulation. Fig. 16 shows a close-up of the temperature distribution inside the Pt probe. Along the probe front surface where spray impinges, the temperature is nonuniform, as it increases towards the heated inner perimeter of the probe. The difference between the maximum and minimum temperatures is around 48 °C.

The model has been demonstrated to be able to quantify heat transfer in this apparatus to extract the local spray heat removal. The steady-state version of this model/measurement system has recently been applied to quantify steady heat transfer in air-mist cooling as a function of water and air flow rates, temperature, water droplet velocity, and size distribution [31,32]. Significant differences in heat removal were observed between transient and steady-state conditions, including temperature hysteresis effects. Future applications of the new system include investigation of (1) the effect of probe temperature, material, and location/orientation relative to the nozzle on the local heat removal, (2) the influence of surface roughness/scale layers and water composition (salt-content, etc.), and (3) quantifying the heat transfer achieved by commercial nozzles used in spray cooling during continuous casting of steel and aluminum for realistic transient conditions found in the plant.

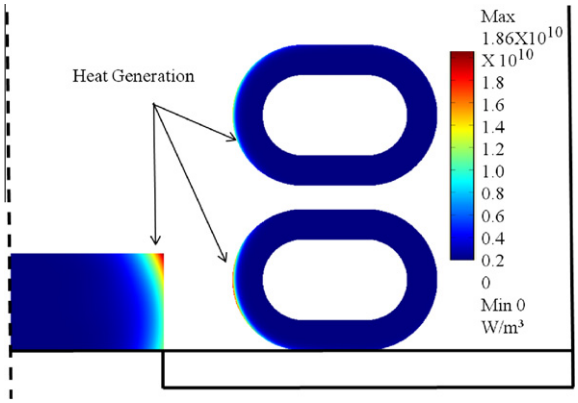

Fig. 14. Heat source power distribution inside the Pt probe and the copper coil.

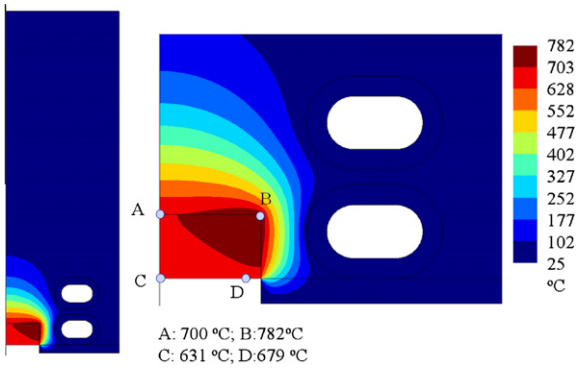

Fig. 15. Temperature distribution in heat transfer domain.

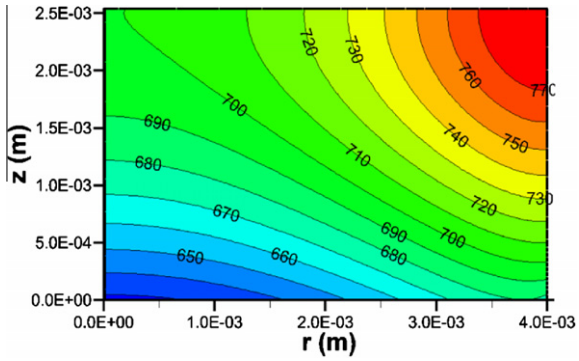

Fig. 16. Temperature distribution in Pt probe (°C).

7. Summary

In this work, a methodology to measure controlled transient heat transfer during spray cooling has been developed by combining a novel induction-heating apparatus with a two-dimensional, axisymmetric computational model of the experiment. The apparatus applies induction heating to a small Pt disk-shaped probe that is controlled to follow a specified temperature history, while being spray-cooled at a given location from the nozzle for various cooling conditions. The model solves the electromagnetics equation and the transient heat-conduction equation using COMSOL. It includes both induction and resistance heating sources to quantify the complete thermal state of the system, including heat removed by the spray water. Separate experiments are conducted to calibrate the temperature-dependent thermal conductivity of the ceramic and other model parameters. Finally, the system is applied to measure the maximum local heat transfer rates during steady-state air-mist spray cooling with a typical commercial nozzle used in continuous-casting of steel.

Acknowledgement

The authors gratefully thank National Science Foundation (Grant #CMMI 09-00138) and the Continuous Casting Consortium at the University of Illinois at Urbana-Champaign for financial support, as well as to the National Council of Science and Technology of Mexico (CONACYT, Grant # 57836).

References

[1] A. Moriyama, K. Araki, T. Okouchi, Heat transfer from hot metal surface to an impinging water droplet in transitional boiling regime, Trans. ISIJ 25 (1985) 198–203.
[2] W. Timm, K. Weinzierl, A. Leipertz, Heat transfer in subcooled jet impingement boiling at high wall temperatures, Int. J. Heat Mass Transfer 46 (2003) 1385–1393.
[3] J. Horsky, M. Raudensky, Measurement of heat transfer characteristics of secondary cooling in continuous casting, Metal 2005, May 24–26, 2005, 14th Internat. Metall. & Material Conf., Czech, Hradec nad Moravici, Tanger, pp. 1–8
[4] M. Raudensky, J. Horsky, Secondary cooling in continuous casting and leidenfrost temperature effects, Ironmaking Steelmaking 32 (2) (2005) 159–164.
[5] M. Raudensky, Heat transfer coefficient estimation by inverse conduction algorithm, Int. J. Numerical Methods Heat Fluid Flow 3 (3) (1993) 257–266.
[6] K. Choi, S. Yao, Mechanisms of film boiling heat transfer of normally impacting spray, Int. J. Heat Mass Transfer 30 (2) (1987) 311–318.
[7] S. Kumagai, Y. Sano, T. Kamata, S. Suzuki, R. Kubo, Boiling heat transfer to an impinged jet in cooling a hot metal slab, Trans. Jpn. Soc. Mech. Eng. B 60 (570) (1994) 609–613.
[8] N. Sozbir, Y. Chang, S. Yao, Heat transfer of impacting water mist on high temperature metal surfaces, J. Heat Transfer 125 (2003) 70–74.
[9] J. Bernardin, I. Mudawar, Film boiling heat transfer of droplet streams and sprays, Int. J. Heat Mass Transfer 40 (11) (1997) 2579–2593.
[10] J. Bernardin, I. Mudawar, Transition boiling heat transfer of droplet streams and sprays, J. Heat Transfer 129 (Nov. 2007) 1606–1610.
[11] K. Graham, S. Ramadhyani, Experimental and theoretical studies of mist jet impingement cooling, J. Heat Transfer 118 (1996) 343–349.
[12] F. Puschmann, E. Specht, J. Schmidt, Measurement of spray cooling heat transfer using an infrared-technique in combination with the phase-doppler technique and a patternator, Int. J. Heat Technol. 19 (2001) 51–56.
[13] J. Schmidt, H. Boye, Influence of velocity and size of the droplets on the heat transfer in spray cooling, Chem. Eng. Tech. 24 (3) (2001) 255–260.
[14] H. Robidou, H. Auracher, P. Gardin, M. Lebouché, L. Bogdanić, Local heat transfer from a hot plate to a water jet, Heat Mass Transf. 39 (2003) 861–867.
[15] J. Donea, S. Giuliani, A. Philippe, Finite elements in the solution of electromagnetic induction problems, Int. J. Numerical Methods Eng. 8 (1974) 359–367.
[16] Ch. Marchand, A. Foggia, 2D finite element program for magnetic induction heating, IEEE Trans. Magn. 19 (6) (1983).
[17] K.F. Wang, S. Chandrasekar, H.T.Y. Yang, Finite-element simulation of induction heat treatment, J. Mater. Eng. Perform. 1 (1) (1992).
[18] C. Chaboudez, S. Clain, R. Glardon, D. Mari, J. Rappaz, M. Swierkosz, Numerical modeling in induction heating for axisymmetric geometries, IEEE Trans. 33 (1) (1997) 739–745.
[19] F. Bay, V. Labbé, Y. Favennec, J.L. Chenot, A numerical model for induction heating process coupling electromagnetism and thermomechanics, Int. J. Numerical Methods Eng. 58 (2003) 839–867.
[20] S.-M. Jang, S.K. Cho, S–H. Lee, H.W. Cho, H.Ch. Park, Thermal analysis of induction heating roll with heat pipes, IEEE Trans. Magn. 39 (5) (2003).
[21] M. Tavakoli, H. Karbaschi, F. Samavat, Computational modeling of induction heating progress, Progr. Electromagn. Res. Lett. 11 (2009) 93–102.
[22] J. Yuan, J. Kang, Y. Rong, R. Sisson, FEM modeling of induction hardening process in steel, J. Mater. Eng. Perform. 12 (5) (2003).
[23] M. Zlobina, B. Nacke, A. Nikanorov and S. Galunin, Numerical Modeling of an Innovative Induction Heating Technique for Aluminum Extrusion Process, in: Proceedings of IFOST-2008-3rd International Forum on Strategic Technologies, 2008, pp. 487–491.

[24] Couple-Field Analysis Guide, 3.5.1. Sample Induction-Heating Analysis of a Circular Billet, ANSYS 11.0 Documentation, pp. 132–139.
[25] COMSOL Multiphysics, AC/DC Module. Available from: <http://www.comsol.com/products/acdc/>.
[26] C. Hernández, X. Zhou, A.H. Castillejos, F.A, Acosta and B.G. Thomas, A Novel Steady-State Technique for Measuring the Heat Extracted by Secondary Cooling Sprays, AISTech 2010 Steelmaking Conference Proc, May 3–6, Pittsburgh, Pa., USA, Assoc. Iron Steel Tech., Warrendale, PA, USA, 2010, pp. 81–92.
[27] L.C. Burmeister, Convective Heat Transfer, second ed., Wiley, New York, 1993. p. 484.
[28] T. Nozaki, J. Matsuno, K. Murata, H. Ooi, M. Kodama, A secondary cooling pattern for preventing surface cracks of continuous casting slab, Trans. Iron Steel Inst. Jpn. 18 (6) (1978) 330–338.
[29] Available from: <http://www.platinummetalsreview.com>.
[30] X. Zhou, Heat Transfer during Spray Water Cooling Using Steady Experiments, Master's Thesis, University of Illinois at Urbana-Champaign, 2009.
[31] C.A. Hernández B., A.H. Castillejos E., F.A. Acosta G., X. Zhou, B.G. Thomas, Measurement of heat flux in dense air-mist cooling: Part I. A novel steady-state technique, Exp. Therm. Fluid Sci. (2012), http://dx.doi.org/10.1016/j.expthermflusci.2012.06.015.
[32] C.A. Hernández B., A.H. Castillejos E., F.A. Acosta G., X. Zhou, B.G. Thomas, Measurement of heat flux in dense air-mist cooling: Part II. The influence of mist characteristics on steady-state heat transfer, Exp. Therm. Fluid Sci. (2012), http://dx.doi.org/10.1016/j.expthermflusci.2012.06.007.